



137  
998  
THS

THESIS

1

2004

57312804

This is to certify that the  
thesis entitled

SELF-ASSEMBLED, FUNCTIONAL PARTICLE  
MONOLAYERS ON POLYELECTROLYTE MULTILAYERS  
FOR OPTICAL COATINGS AND DIFFUSE REFLECTORS

presented by

Jin Soo Ahn

has been accepted towards fulfillment  
of the requirements for the

Master of  
Science

degree in

Chemical Engineering and  
Materials Science

  
\_\_\_\_\_  
Major Professor's Signature

5/11/2004

Date



**SELF-ASSEMBLED, FUNCTIONAL PARTICLE MONOLAYERS ON  
POLYELECTROLYTE MULTILAYERS FOR OPTICAL COATINGS AND DIFFUSE  
REFLECTORS**

**By**

**Jin Soo Ahn**

**A THESIS**

**Submitted to  
Michigan State University  
in Partial Fulfillment of the Requirements  
for the Degree of**

**MASTER OF SCIENCE**

**Department of Chemical Engineering and Materials Science**

**2004**

## ABSTRACT

### SELF-ASSEMBLED, FUNCTIONAL PARTICLE MONOLAYERS ON POLYELECTROLYTE MULTILAYERS FOR OPTICAL COATINGS AND DIFFUSE REFLECTORS

By

Jin Soo Ahn

Monolayers of charged polystyrene latex particles ranging in size from 100 nm to 10  $\mu\text{m}$  were deposited onto oppositely charged polyelectrolyte multilayers (PEMs) by electrostatic interactions. Ultrathin PEMs ( $\sim 30$  nm) formed on a glass slide provided an excellent underlying adhesive layer. As the sample surface was being dried, strong capillary forces between particles resulted in a unique pattern of 2-D particle monolayers. The resulting topographically structured coatings strongly influenced visible light transmission through the slides, resulting in three different characteristics as a function of particle size: (1) anti-reflection, when the particle diameter ( $D_{\text{particle}}$ ) is around a quarter of the wavelength of the incident light ( $D_{\text{particle}} \sim \lambda/4$ ), (2) diffraction when  $D_{\text{particle}} \sim \lambda$ , and (3) diffusive scattering when  $D_{\text{particle}} > \lambda$ . Functional groups present in these novel coatings allow further customization via chemical modification. The particle coated samples were further modified using electroless nickel plating technique. Created surfaces are diffusive metal reflectors with controlled roughness. A UV-VIS spectrometer with fiber optics was employed to characterize the optical properties of the reflectors. Optical measurements showed that the proposed method could control the ratio of specular and diffuse reflection among total reflected light by changing particle size only. This novel method is simple, cost-effective and appropriate for mass production because the process consists of simple immersion steps without vacuum technology or special devices.

## ACKNOWLEDGMENTS

I would like to first thank my wife for her love and care. I wish to thank my academic advisor, Dr. Ilsoon Lee, without whom none of this work would have been finished, for his support and insightful guidance through two years of study. I also would like to thank the other members of my graduate committee, Dr. Andre Lee and Dr. Patrick Kwon. I also wish to thank my friend, Tim Wong, for giving me his time and advice in the calculation of the light distribution. I would like to thank the colleagues with whom I spent most of graduate works, Troy Hendricks, Srivatsan Kidambi, Neeraj Kohli and Brian Hassler. Finally, I would like to thank my parents for all of their support and love throughout the years.

The analytical support is provided through the Surface Characterization Facility in the Composite Materials and Structures Center at Michigan State University is gratefully acknowledged. This work was funded by the MSU Start-Up Funds and the Seed Research Fund by the Center for Fundamental Materials Research at MSU.

## TABLE OF CONTENTS

LIST OF TABLES.....	v
LIST OF FIGURES.....	vi
1. BACKGROUND.....	1
2. PARTICLE MONOLAYERS AS OPTICAL COATINGS.....	4
2.1 Introduction.....	4
2.2 Experimental Procedures.....	4
2.3 Results and Discussion.....	8
2.3.1 Formation of Particle Monolayers on PEMs.....	8
2.3.2 Structure of Self-Assembled Particle Monolayers on PEMs.....	11
2.3.3 Light Transmittance of Particle Coated Samples.....	13
2.4 Conclusions.....	20
3. PARTICLE MONOLAYERS AS DIFFUSE REFLECTORS.....	22
3.1 Introduction.....	22
3.2 Experimental Procedures.....	24
3.2.1 Electroless Plating of Particle Monolayers.....	24
3.2.2 Optical Characterizations of Diffuse Reflectors.....	24
3.3 Results and Discussion.....	27
3.3.1 Formation of Nickel Plated Particle Monolayers.....	27
3.3.2 Optical Characterizations of Diffuse Reflectors.....	29
3.4 Conclusions.....	32
4. SUMMARY AND CONCLUSIONS.....	34
5. BIBLIOGRAPHY.....	36

## LIST OF TABLES

Table 1: Details of Particles Used and Their Monolayers.....	6
Table 2: Ratio of Specular and Diffuse Reflection.....	31

## LIST OF FIGURES

Figure 1: Measurement Schematics for the Total and Specular Transmittance.....	8
Figure 2: SEM Image of Self-Assembled Particle (140 nm) Monolayer.....	9
Figure 3: SEM Image of Self-Assembled Particle (0.5 $\mu\text{m}$ ) Monolayer.....	9
Figure 4: Microscopic Image of Self-Assembled Particle (4 $\mu\text{m}$ ) Monolayer.....	10
Figure 5: Total Transmittance.....	14
Figure 6: Specular Transmittance.....	15
Figure 7: Antireflective Coating.....	16
Figure 8: Diffractive Coating.....	18
Figure 9: Diffusive Scattering Coating.....	20
Figure 10: Reflectivity of Metals.....	23
Figure 11: Measurement Schematic for the Specular and Diffuse Reflectance.....	25
Figure 12: Measurement Schematics for the Angular Dependent Reflectance.....	26
Figure 13: SEM Image of a Nickel-Plated 140 nm Particle Monolayer.....	27
Figure 14: SEM Image of a Nickel-Plated 0.5 $\mu\text{m}$ Particle Monolayer.....	28
Figure 15: Optical Microscopic Image of Nickel-plated 3 $\mu\text{m}$ Particle Monolayer.....	29
Figure 16: Specular and Diffuse Reflectance.....	30
Figure 17: Distribution of Reflected Light.....	31
Figure 18: Macroscopic View of Reflectors at Different Angles.....	32

# 1. BACKGROUND

Studies of colloidal particle assembly at surfaces have provided fundamental insight into colloidal behavior and aggregation, and suggested potential applications such as optical band gap materials and coatings. Ordered, three-dimensional (3-D) colloidal multilayers have been investigated as optical filters and photonic crystals<sup>1-8</sup>. Two-dimensional, (2-D) colloidal assemblies have been investigated for applications including anti-reflection (AR) coatings<sup>9</sup>, gratings<sup>10</sup>, interferometers<sup>11</sup>, photolithographic masks<sup>12-14</sup>, and optical coatings<sup>15</sup>. Recent developments in 2-D particle assemblies include the positioning of particles on desired surface spots<sup>16-21</sup> and incorporation of molecular and colloidal materials into spatial patterns<sup>7,15,22</sup>.

2-D particle monolayers assembled on surfaces can be categorized as either densely close-packed or randomly adsorbed. Densely close-packed particle monolayers have been fabricated using spin coating<sup>23</sup>, Langmuir Blodgett (LB)-techniques<sup>24</sup>, thin laminar flow liquid film<sup>25</sup>, monolayer transfer<sup>13</sup>, and electrophoretic deposition<sup>26</sup>. Although these methods have successfully produced hexagonally packed particle arrays, they were weakly adsorbed on the substrate, and tedious to perform or required specific devices; in addition, long-range ordering has been a problem for the practical applications. Evaporation methods are simple and widely used in making densely packed particle monolayers<sup>27</sup>, but the size of ordered regions produced has been limited. To achieve close packing over a larger area, additional control is required (e.g., tilting samples in the evaporation process<sup>14</sup>).

On the other hand, fabrication of randomly dispersed monolayers via

electrostatic attractive forces between the particles and the substrate is relatively easy and does not require special devices<sup>9,28-33</sup>. The properties of randomly dispersed monolayers depend on particle dispersion and clustering tendencies. Lateral capillary forces help form ordered regions by convective flow during solvent evaporation but the particles are repulsive to each other<sup>27,34,35</sup>. When the capillary force is greater than the repulsive force, monolayers exhibit random-close-packed (RCP) particle clusters that contain branch-like structures of interconnected and/or hexagonally packed particles. Among various random deposition methods, electrostatic deposition using polyelectrolyte multilayers (PEMs) as an ultrathin adhesive layer has advantages of being simple to perform, cost-effective, and environmentally friendly. PEMs are formed in the layer-by-layer assembly process, which consists of the sequential alternating immersion of a substrate into polycation and polyanion solutions to construct a nanostructured ultrathin film. Charged particles can then be deposited via electrostatic interactions to form monolayers atop the PEM.

Layer-by-layer electrostatic assembly of PEM, originally developed by Decher<sup>36,37</sup>, has been widely studied because of its versatility and potential applications. Fabrication of nanostructured PEM films is simple and can be successfully achieved without the need for a clean-lab facility<sup>38,39</sup>. The PEMs can be formed on flat, curved, and even spherical surfaces (e.g., a colloidal particle)<sup>7,40,41</sup>. Additionally, PEMs contain multiple functional groups that can serve as molecular templates for further customization. Dendrimers, proteins, inorganics, and micro-/nano-particles have been co-assembled into PEM<sup>42-57</sup>.

Inspired by the report that specifically sized particle monolayer on adhesive layer

of PEM provided simple and cost-effective AR coating<sup>9</sup>, we expanded the study of light transmittance by colloidal monolayers using variously sized colloidal particles. Details of transmitting properties of colloidal monolayers and corresponding optical coating applications will be discussed in Chapter 2.

One of good advantage in using this approach for optical coatings is the coatings are still available for further modifications for various applications. In this work the coatings were further modified with nickel by a two-step electroless plating using palladium catalysts. Resulting surfaces are rough metal controlled by particle sizes suggesting a novel method of creating a diffusive metal reflector application. For the characterization of optical properties a UV-VIS spectrometer with fiber optics was employed. Optical fibers permit versatile and precise measurements of specular and diffuse reflectance and angular dependent reflectance. Also, we demonstrate how to estimate the distribution of reflected light from the surface and the ratio of specular and diffuse reflection among the total reflected light using angular dependent reflectance. Optical measurements showed that this approach could control the portion of the diffuse reflection from 8.25 to 59.97 %. Proposed method is simple, cost-effective and apt for mass production because the process consists of simple immersion steps without vacuum technology or special devices.

## 2. PARTICLE MONOLAYERS AS OPTICAL COATINGS

### 2.1 Introduction

Hideshi demonstrated that monolayers of silica and polymeric nanoparticles ( $D_{\text{particle}} \sim 1/4\lambda$ ) yield an anti-reflective AR coating effect<sup>9</sup>, while many others have investigated 2-D or 3-D microparticle monolayers or multilayers ( $D_{\text{particle}} \sim \lambda$ ) for photonic and band gap materials<sup>58,59</sup>. We have formed polystyrene (PS) particle monolayers via electrostatic interactions between charged particles and oppositely charged PEM surfaces. The structure and optical properties of these coatings are controlled by electrostatic interactions and capillary forces<sup>15,33</sup>.

While the optical properties of colloidal multilayers and close-packed monolayers have been extensively studied, those of randomly adsorbed or RCP monolayers have not. In this study, we systematically investigated RCP produced by electrostatically adsorbing PS particles between 100 nm and 10  $\mu\text{m}$  in diameter onto PEM-coated glass slides. Surface coverage and fractal dimensions of the RCP monolayers were measured using image analysis, and the optical properties were studied using both total and specular transmittance. The possibility of modeling RCP monolayers based on the 2-D coverage and fractal dimension analysis using a box-count method was also considered<sup>60</sup>.

### 2.2 Experimental Procedures

Poly(diallyldimethylammonium chloride) (PDAC) and sulfated polystyrene (SPS) were purchased from Aldrich. Average molecular weights of PDAC and SPS were

~100,000 – 200,000 and 70,000, respectively. Microscope glass slides were ordered from Corning and used as transparent substrates for PEMs and particle coatings. All aqueous solutions in the process were prepared using deionized (DI) water ( $>18.1 \text{ M}\Omega$ ) supplied by a Barnstead Nanopure Diamond-UV purification unit equipped with a UV source and final  $0.2 \mu\text{m}$  filter.

Glass slides were first cleaned twice in an ultrasonic unit, first with a commercially available detergent (Alconox, Alconox Inc.) and then without. Slides were dried under a  $\text{N}_2$  gas stream and then treated with oxygen plasma for 10 minutes at 150 millitorr vacuum to activate negative surface charges on the glass.

Aqueous polyelectrolyte solutions were prepared containing either 20 mM PDAC or 10 mM SPS in 0.1 M NaCl. PDAC/SPS bilayers were then deposited by sequential immersion of the glass slides into the two solutions using a Microm DS 50 Slide Stainer purchased from Richard-Allan Scientific. PDAC was deposited first, because its positively charged amine groups bind to the negatively charged hydroxyl groups of glass. In each step, the slides were immersed in a polyelectrolyte solution for 20 minutes, followed by two 5-minute rinses in DI water. After each PDAC/SPS bilayer was deposited, the slides were immersed in an ultrasonic bath for 1 minute to remove loosely attached polyelectrolyte. This sequence was repeated until  $(\text{PDAC/SPS})_{10.5}$  bilayers were formed.  $(\text{PDAC/SPS})_{10.5}$  bilayers have a positive PDAC top layer, which is needed to electrostatically bind the negatively charged PS particles. Substrates were finally dried under a  $\text{N}_2$  gas stream and stored for particle coating.

The sulfate-functionalized and carboxylic-acid-functionalized PS particles were obtained from Interfacial Dynamics Corp., and Polysciences, Inc., respectively. Size-

distribution and surface-charge density information obtained from the manufacturers is shown in Table 1.

Table 1. Details of Particles Used and Their Monolayers

Particle Size ( $\mu\text{m}$ )	Size Distribution Diameter $\pm$ SD ( $\mu\text{m}$ )	Surface Functional Group	Surface Charge Density ( $\mu\text{eq/g}$ )	Monolayer Coverage by particles $\pm$ SD (%)	Fractal Dimension, $D_f$
0.14	0.14 $\pm$ 0.003	Sulfate	3.4	32.60 $\pm$ 1.803	1.778
0.2	0.194 $\pm$ 0.009	Carboxylate	100-200	N/A	N/A
0.5	0.477 $\pm$ 0.01	Carboxylate	100-200	40.38 $\pm$ 9.928	1.799
1	1.0 $\pm$ 0.047	Sulfate	83.9	39.40 $\pm$ 0.809	1.804
2	1.96 $\pm$ 0.06	Carboxylate	100-200	39.36 $\pm$ 1.377	1.800
3	3.00 $\pm$ 144	Carboxylate	100-200	54.20 $\pm$ 1.684	1.828
4	4.0 $\pm$ 0.14	Sulfate	0.8	59.36 $\pm$ 2.853	1.848
5	4.9 $\pm$ 0.275	Sulfate	0.5	47.44 $\pm$ 6.307	1.846
8	7.9 $\pm$ 0.845	Sulfate	0.4	67.38 $\pm$ 18.709	1.826
10	9.6 $\pm$ 0.710	Sulfate	1 <sup>2</sup>	65.14 $\pm$ 19.656	1.835

To bind PS particles to the PEM, a 0.5 wt % colloidal solutions was gently dropped on the PEM surface. After a 1-hour incubation, the particle-coated substrates were washed carefully with deionized water and dried under a N<sub>2</sub> stream. Microscopic images of the coatings were obtained using a Nikon Eclipse ME600 optical microscope and a JEOL 6400V scanning electron microscope (SEM) with a LaB6 emitter. The degree of surface coverage was determined by counting particles in a given area. Coverage measurements were repeated several times in both particle-rich and particle-

poor regions. Data were reported as average standard deviation values.

Microscopic images were further investigated by fractal analysis using a 2-D box-counting method<sup>60</sup>. All monolayer images were scaled to have the same particle sizes, and each particle was considered as a single point. The maximum number of boxes was 4096. Boxes were counted manually and plotted on logarithmic-scale graph. Fractal dimensions were calculated using a least squares regression method. A UV/VIS/NIR Spectrometer Lambda 900 (Perkin-Elmer) was used to study the optical properties of the samples. Both photomultiplier tube (PMT) and integrating sphere (IS) detectors were used for specular and total transmittance characterization, respectively. All spectroscopic spectra of the samples were referenced against air, without a substrate.

Figure 1 illustrates the difference in measurement principle between the PMT and IS detectors. The IS detector collects all light passing through the substrate regardless of the back scattering angle (Total Transmittance), while the PMT detector only captures light transmitted in the same direction as the incident light (Specular Transmittance). Both detectors scanned transmittance by 1 nm wavelength scale. Transmittance spectra from both detectors were averaged at 400~800 nm wavelength range to compare the size effects on scattering (averaged total and specular transmittances). The total transmittance spectrum of every particle monolayer is not reported, because there was little change in light intensity with wavelength. However, all specular transmittance spectra are presented and categorized into 3 groups, depending on the optical behavior.

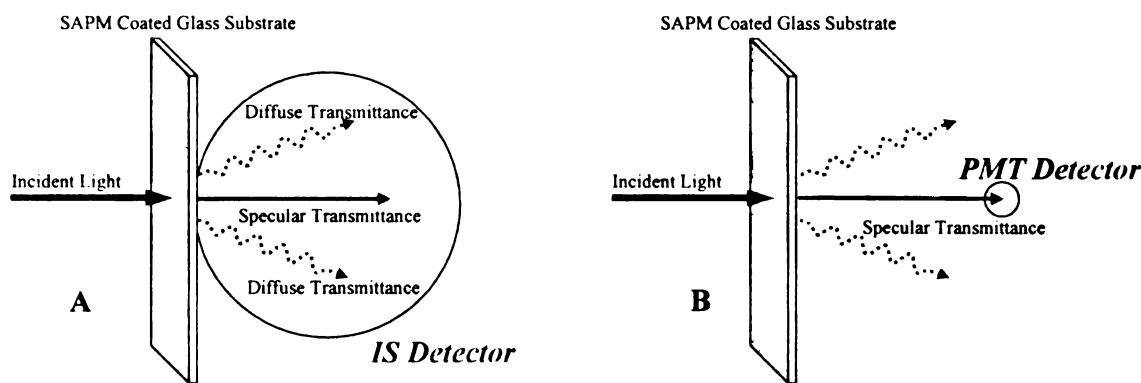


Figure 1: Measurement Schematics for the Total and Specular Transmittance

## 2.3 Results and Discussion

### 2.3.1 Formation of Particle Monolayers on PEMs

Figure 2, 3, and 4 show the SEM and optical microscope images of the particle monolayers assembled on the (PDAC/SPS)<sub>10,5</sub>-coated glass slides. Particles forming multilayers on top of the first adsorbed particle layer were easily washed away during the rinsing steps because of the repulsive forces with the first layer of identically charged particles. The layer of particles is strongly adhered to the surface by electrostatic attraction forces between negatively charged colloidal particles and the positively charged PDAC top surface of the PEMs.

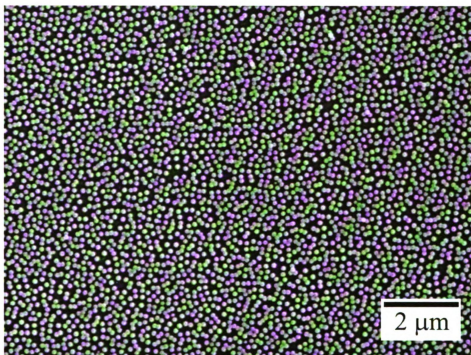


Figure 2: SEM Image of Self-Assembled Particle (140 nm) Monolayer

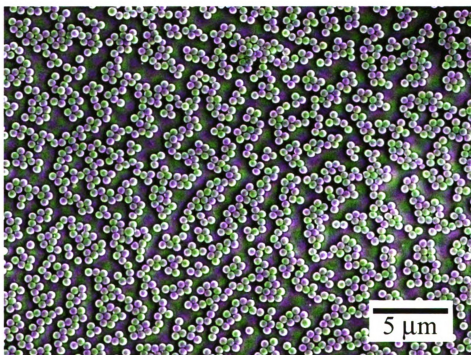


Figure 3: SEM Image of Self-Assembled Particle (0.5 μm) Monolayer

Functional nanospheres (140 nm) are well dispersed and deposited independently on the surface (Figure 2); whereas the larger microspheres (0.5  $\mu\text{m}$  – 10  $\mu\text{m}$ ) also formed two-dimensional monolayers but have clusters of close packed particles connected with each other, forming fractal-like structures (Figures 3 and 4). The formation of the fractal-like particle monolayers (i.e., RCP monolayer) is obvious for particles bigger than 140 nm. 200 nm-sized particles did not form monolayers even with several trials; instead they formed 2 or 3 layered aggregates. The reason for the formation of the layered aggregates is not clear, but the optical properties were compared with other particle monolayers.

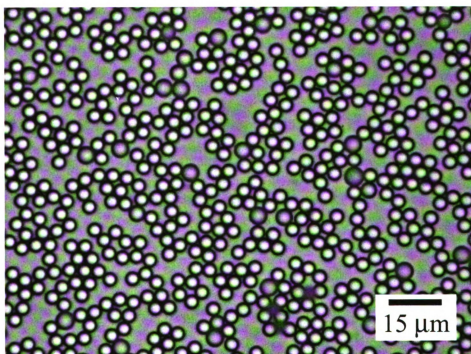


Figure 4: Microscopic Image of Self-Assembled Particle (4  $\mu\text{m}$ ) Monolayer

In the beginning of functional particle depositions in aqueous solution, the negatively charged particles were attracted to the positively charged PEM surfaces until the available PEM surfaces were fully occupied. Then, during the sample drying step

when the water level became comparable to the size of adsorbed particles, a rearrangement of adsorbed particles started to occur, resulting in uniquely self-assembled monolayer patterns on the PEM-coated glass slides, as shown in Figure 3 and 4. During the rearrangement of adsorbed particles near or on the PEM-substrate, two conflicting forces, repulsive and attractive forces, compete to determine the pattern of the self-assembled particle monolayers. The repulsive forces between particles adsorbed on PEM surfaces are due to the same particle charges and the attractive forces are because of capillary forces stimulated from the menisci of water formed around the particles<sup>17</sup>. Repulsive forces hinder the packing of two-dimensional particles while attractive forces help the packing of particles by the convective transport of particles toward the close packed region. We believe that the attractive capillary forces were smaller than the repulsive forces in the case of 140 nm nanospheres, these results in particles that are relatively isolated from each other<sup>61</sup>. This conclusion is supported by the fact that particle closed packing can be obtained by reducing electrostatic repulsive forces between particles using surfactant charge screening<sup>62</sup>. For particles larger than 0.5  $\mu\text{m}$ , the capillary forces were dominant at the last stage of drying, resulting in the RCP particle monolayers.

### **2.3.2 Structure of Self-Assembled Particle Monolayers on PEMs**

Table 1 shows physical data of the particles used in this work and monolayer coverage characterized by direct particle counting. The fifth column of Table 1 shows the calculated particle coverage from the microscopic images. Particle coverage was found to be independent of the two different types of charged groups on the particles' surface. Sulfate groups make the surface of the particle hydrophobic, and carboxylate

groups hydrophilic. Both cases showed attractive forces among particles. Particle monolayer coverage was affected more by the size of the particles. The coverage of the particle monolayers generally increased with increase in the size of the particles. This is because the particle clustering, due to the increased capillary forces among particles, increased with the increase in particle size. The surface coverage did not reach a theoretical maximum because monolayers created by this method cannot form a close-packed monolayer. The calculated maximum surface coverage by spherical objects is 90.69% when they are hexagonally packed.

When particles are strongly attached to the substrate, the diffusion process or surface migration of particles is hindered and there is a limit for coverage known as the jamming limit of random sequential adsorption (RSA)<sup>63,64</sup>. 54.7% is in good agreement for the maximum coverage by this model<sup>63,64</sup>. However, RCP monolayers with particles greater than 2  $\mu\text{m}$  have coverages greater than this limit (Table 1). This means there is movement and diffusion of particles during deposition and evaporation which allow the particles to surpass the jamming limit. The structure of colloidal aggregates formed in this process is a fingerprint of the kinetics and mechanism of aggregation. Simple aggregation models and real aggregation processes frequently lead to fractal structures that can be described in terms of fractal geometry concepts<sup>65</sup>. Fractal geometry, also known as the fractal dimension, enables us to relate certain aggregates to a proper kinetic and growth mechanism model<sup>66</sup>. In two-dimensional analysis, the fractal dimension has a value between one and two. When fractal geometry completely fills a certain area of the surface, the fractal dimension reaches the maximum value of 2.

We calculated the fractal dimensions of our samples in an effort to find a proper

model to explain the uniquely self-arranged particle monolayers on PEMs. The last column of Table 1 presents the calculated 2-D fractal dimensions,  $D_f$ , of each sample. Fractal dimensions of RCP monolayers range from 1.778 to 1.848. The aggregation shape of the RCP model closely resembles that of cluster-cluster aggregation by primary clusters. There are two different mechanisms for this type of aggregation, ‘reaction-limited cluster-cluster aggregation’ (RLCCA) and ‘diffusion-limited cluster-cluster aggregation’ (DLCCA)<sup>67</sup>. When there is a diffusion process during the aggregation and the particle adsorption is instant compared with the diffusion time, the ‘diffusion-limited-aggregation’ (DLA) model can explain the process. On the other hand, an aggregation process with residual repulsive forces between particles can be explained by the ‘reaction-limited-aggregation’ (RLA) model<sup>68</sup>. It is known that the fractal dimension of RLCCA is higher than that of DLCCA<sup>67</sup>. A high fractal dimension of RCP monolayer indicates its close relationship with the RLCCA model. However, relating the aggregate structure to a specific growth mechanism is not fully understood yet. As is the problem with modeling all colloidal aggregations, modeling RCP monolayers using a specific model is very challenging and needs further studies. However, one thing that remains clear is that the capillary forces that occur during the sample drying step play a very important role in the resulting RCP monolayers on PEMs which are very similar to the description by the RLCCA model.

### **2.3.3 Light Transmittance of Particle Coated Samples**

Figure 5 shows the average total transmittance of the samples at the visible light range (400~800 nm), which was measured using an UV/Vis spectrometer equipped with an IS detector. No significant reflection or absorption by the coated polystyrene particle

monolayer has been found in this work. The average total transmittances, ranging from 90.06 % to 94.12 %, remained very high and are comparable to the values of a pure glass slide. The average transmittance of a pure glass slide measured by the same IS detector was 91.86 % at the same wavelength range. This implies that the particle monolayer coatings did not affect the total transmittance of the glass slides. Also, there is no significant particle size effect on the observed total transmittance.

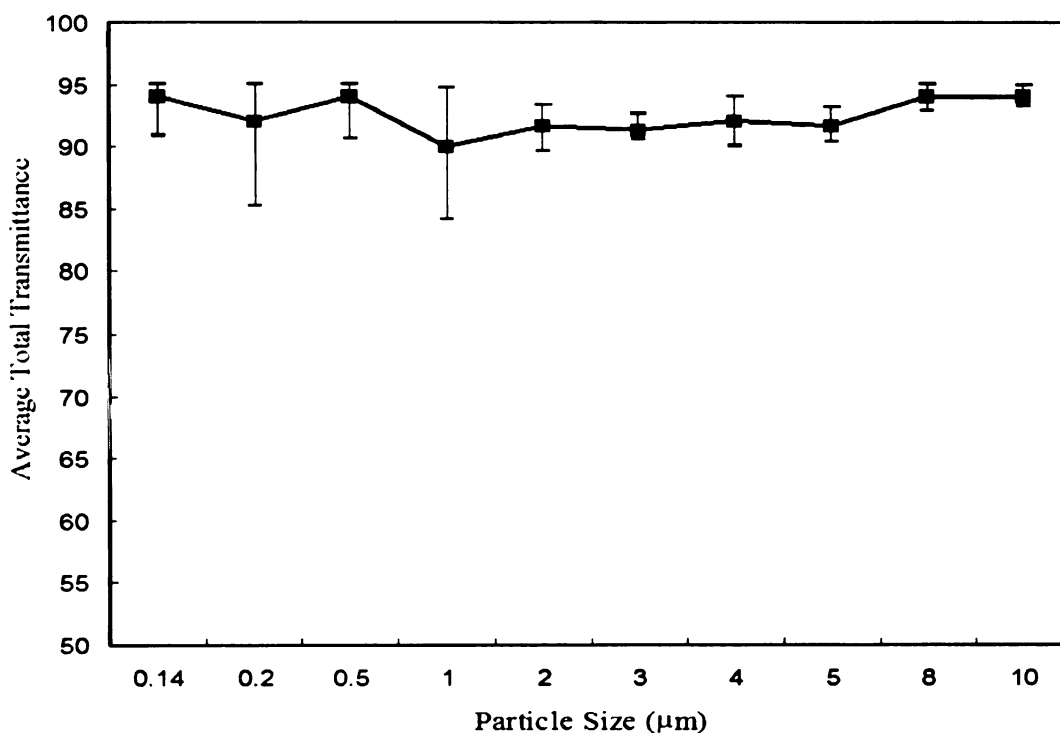


Figure 5: Total Transmittance

Figure 6 shows the averaged specular transmittance measured using a PMT detector. The specular transmittance varies with the size of particle. A decrease in the specular transmittance compared to the observed total transmittance of the same sample indicated that some portion of incident light did not reach the detecting point because of a ‘scattering event’. Monolayers of particles bigger than  $0.5 \mu\text{m}$  yielded an ‘apparent

scattering' event when incident visible light passed through the particle coated glass slides. Apparent scattering happens when the size of the scattering particle is equal to or greater than the wavelength of incident radiation<sup>69</sup>. Particle coated glass slides with 140 and 200 nm sized particles did not exhibit significant scattering events. The samples looked either transparent without scattering events or translucent with those scattering events, depending on the size of particles.

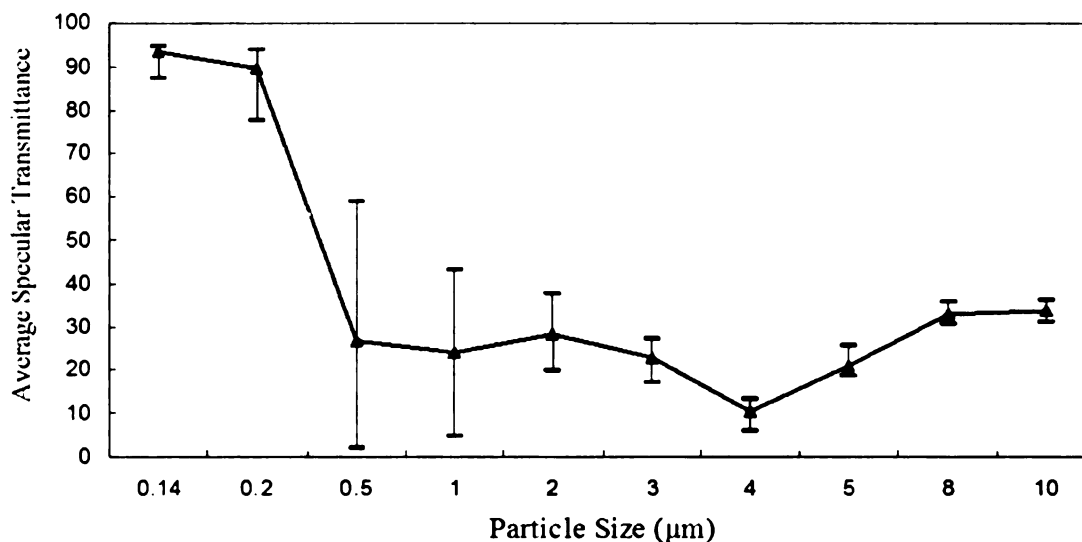


Figure 6: Specular Transmittance

Figure 7, 8, and 9 shows the specular transmittance spectra from a uv/vis-spectroscopy experiment using a PMT detector, which was not averaged. There are three main observed behaviors which are dependent on the particle size: Anti-reflection behavior for the particles ranging in size from 0.14 to 0.2 micrometers (Figure 7), diffraction for the particles ranging in size from 0.5 to 4 micrometers (Figure 8), and diffusive scattering for the particles ranging in size from 5 to 10 micrometers (Figure 9).

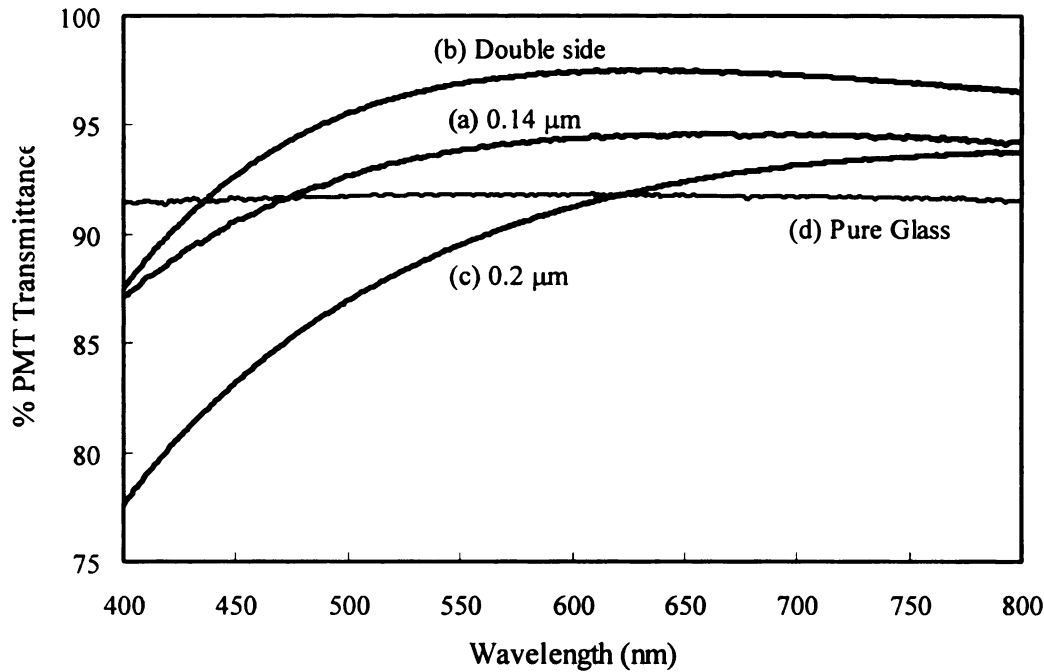


Figure 7: Antireflective Coating

Figure 7 shows the transmittance spectra using a PMT detector in the visible light range, 400 ~ 800 nm. Particles with diameters of 140 and 200 nm have an AR behavior and exhibit an enhanced transmittance that is greater than that of a pure glass. Glass slides coated with particles on both sides have a higher transmittance than those coated on a single side. The maximum value of transmittance for this particle size was measured to be 97.52 % at a wavelength of 635 nm, which is much higher than that of the pure glass slide (c.a., 92 %).

To be an AR coating, the designed film should satisfy two conditions<sup>70</sup>. The thickness of the AR coating must be a quarter of the incident wavelength and  $n_c = (n_a n_s)^{1/2}$ , where  $n_c$ ,  $n_a$  and  $n_s$  are the refractive indices of the coating, air, and substrate, respectively. Anti-reflective behavior is due to the destructive interference between reflected lights

from the top surface of AR coating and from the interface between the AR coating and substrate. Also,  $n_c$  must have a value between  $n_a$  and  $n_s$  so that the change in refractive indices of the media is gradual and reduces the amount of light reflecting backwards from the substrate.

The particle coatings produced with 140 and 200 nanometers sized particles satisfy both conditions for an AR coating. The thickness of these monolayers is directly decided by the diameters of the particles, which is around a quarter of the visible light wavelengths. Refractive indices of air, glass, and polystyrene particles are generally 1, 1.5, and 1.59 (data from Interfacial Dynamics Corp.), respectively. Due to the random deposition of particles, the monolayer has many pores between polystyrene particles that are filled with air. The monolayer has a refractive index somewhere in between that of air and polystyrene particles. As illustrated by Hideshi<sup>9</sup>, this approach to forming an AR coating does not require a high vacuum that is common in many AR coating processes. This process is more cost-effective when compared to phase separation or selective dissolution approaches<sup>71</sup> and simpler than vapor deposition or sputtering approaches<sup>72,73</sup>.

Figure 8 shows the oscillating specular transmittance spectra from particles with 0.5, 1, 2, 3 and 4  $\mu\text{m}$ . In the late sixties O'Neill, *et al.*<sup>69</sup>, demonstrated that monodispersed latex particles exhibited diffraction in both colloidal solution and dry particle layers. We believe this diffraction event can be categorized into Fraunhofer diffraction, which occurs when light propagates through an assembly of apertures or translucent screens<sup>70</sup>. This is supported by the fact that there is a typical airy disc created by a circular aperture when the laser from a laser pointer is shined through the samples. However, this airy disc pattern is unclear because the self-assembled particle

monolayers on PEMs are RCP structures. Maxima and minima in the spectra represent the change in intensity with the change in the wavelength of incident monochromatic light.

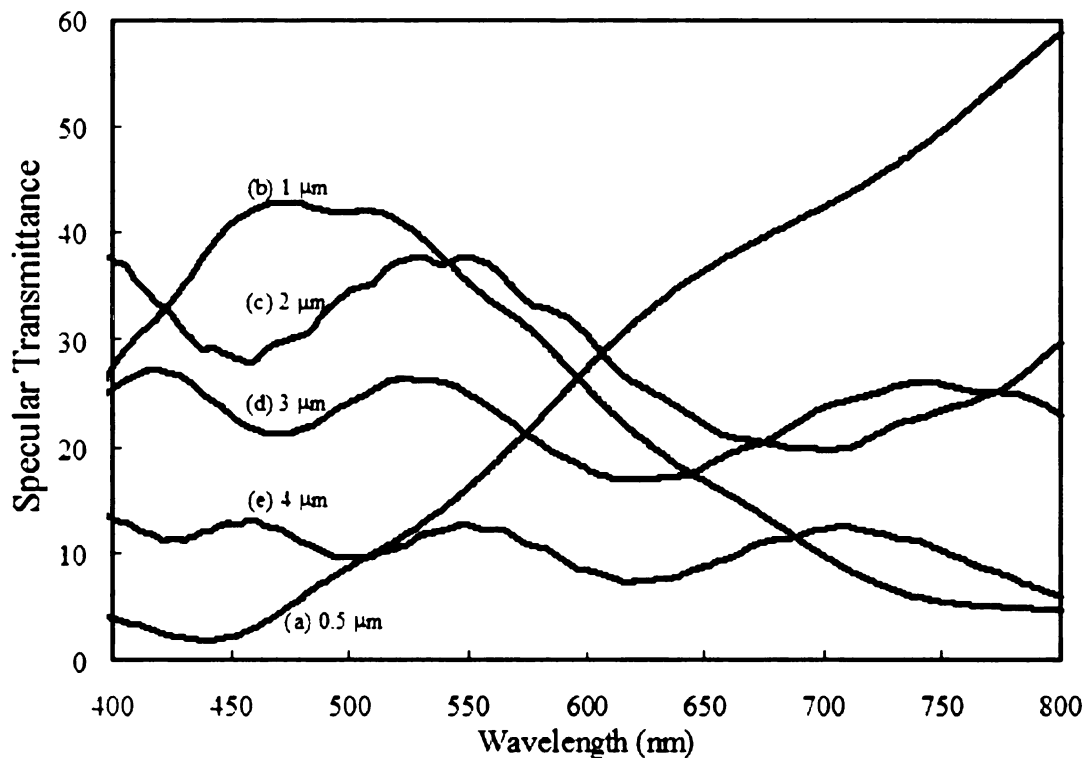


Figure 8: Diffraction Coating

Interesting results from the diffracted transmittance spectra are obtained for monolayers made from 0.5 and 1  $\mu\text{m}$  sized particles. A 0.5  $\mu\text{m}$  sized particle monolayer completely scatters blue light but transmits about 58% of incident red light. To the contrary, a 1  $\mu\text{m}$  sized particle monolayer scatters almost all incident red lights but passes 42 % of incident blue light. By simply changing the size of the particles a particle monolayer can selectively block a specific wavelength.

Current studies on the selective transmission of incident light by diffraction have

U

focused on 3-D colloidal crystals. In this case, sharp peaks at specific wavelengths are exhibited due to the Bragg diffraction through the ordered arrays. Selectivity in the transmission of light in narrow wavelength regions is useful in diffractive components of optical filters or in grating applications<sup>1</sup>. Different from ordered aggregations, RCP monolayers produce broad peaks that are unique in their diffraction through 2-D or 3-D multilayers.

While the details of this diffraction mechanism need to be further studied, we expect that there may be other potential applications in which this broad selective transmission can be very useful. We can further tune the optical selectivity using commercially available fluorescent particles<sup>74</sup>. Additionally, we can control these broad peaks using mixed or polydispersed particle monolayers.

Figure 9 shows the specular transmittance spectra using a PMT detector from particles with diameters of 5, 8 and 10  $\mu\text{m}$ . This group exhibits uniform diffusive scattering of incident light. The transmitted light reaching the PMT detector shows a uniform intensity along the wavelengths. The specular transmittance was decreased when compared to the total transmittance. This means that there happened to be a scattering event that changed the direction of the incident light. Optical coatings of the particle monolayers in this group transmitted diffraction free and uniform light. Once again, it is noted that the total transmittance measured using a IS detector remained almost the same regardless of the particle size. The transmitted light, through the self-assembled monolayers on PEM-coated glass slides, were scattered or diffracted differently depending on the topological surface structures controlled by the size of particles.

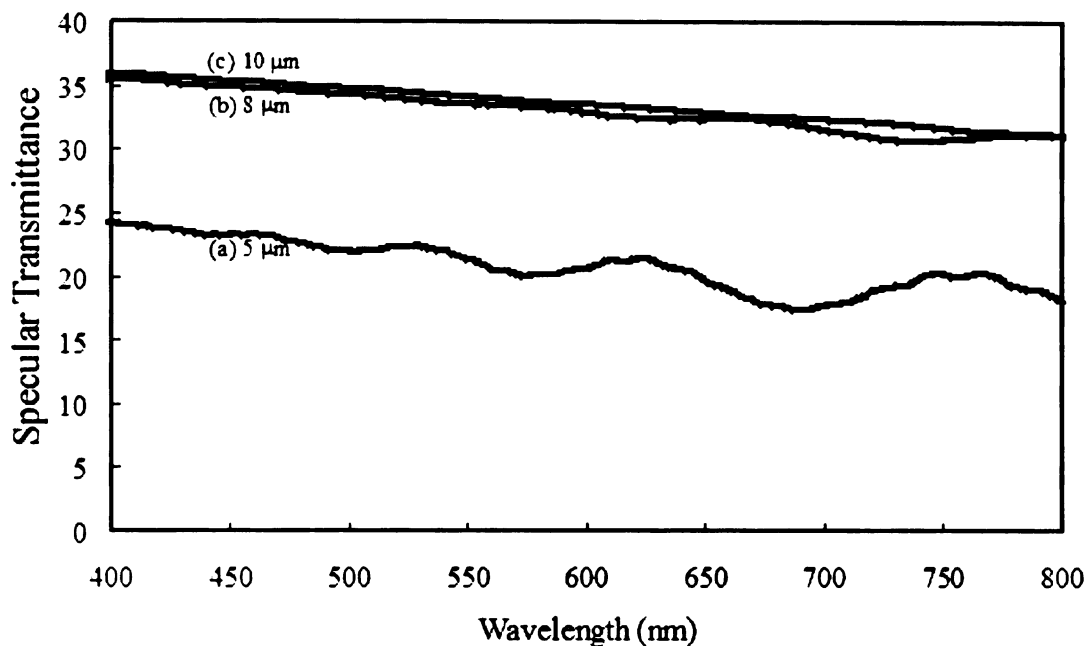


Figure 9: Diffusive Scattering Coating

## 2.4 Conclusions

We have studied the functional PS particle size effects on the formations, structures, and optical properties of the uniquely self-assembled particle monolayers on PEM-coated glass slides. The particles formed RCP monolayers that deposited on the substrate by electrostatic attraction forces and then rearranged by capillary forces among the attached monolayer particles. Compared to other particle deposition approaches, the overall procedure used in this work was very simple, cost-effective, and environment friendly. The formation and structure of the self-assembled particle monolayers (i.e., RCP particle monolayers) was analyzed using surface particle coverage and fractal dimension analysis. The optical properties of the self-assembled particle monolayers measured using two different detectors showed very interesting particle size dependencies. Even though the apparent changes dependent on particle size could be

identified with the bare eye, the total transmittance, measured using an IS detector, remained unchanged and conversely the specular transmittance, measured using a PMT detector, changed considerably. No significant reflection or absorption by the coated monolayer has been found. This indicates that the incident visible light optically interacts with the particle monolayers through optical interference, diffraction, and/or scattering events. Three main optical characteristics as a ratio of particle diameter vs. wavelength of incident beam ( $D/\lambda$ ) are the following: (a) Anti-reflection (when  $D/\lambda \sim 0.25$ ), (b) diffraction (when  $D/\lambda \sim 1$ ), and (c) diffusive scattering (when,  $D/\lambda > 1$ ). These functional and topographically structured surfaces can be further used as templates for selective and non-selective metal plating<sup>75</sup>, cell adhesion<sup>76</sup>, and quantum dot deposition<sup>7</sup>.

### 3. PARTICLE MONOLAYERS AS DIFFUSE REFLECTORS

#### 3.1 Introduction

Diffuse reflectors are widely used in back-light unit of liquid crystal display (LCD) panels<sup>77-79</sup> and solar cell devices<sup>80,81</sup>. A perfect diffuse reflector refers to a matter that reflects incident energy uniformly to all directions and is observable at all viewing angles. The similar characteristics for a practical diffuse reflector can be simply achieved by having topographical roughness on a highly reflective surface, such as metal. A uniformly controlled rough surface reflects incident light in a diffusive manner reducing specular reflection due to the random scattering of light to all directions<sup>82-85</sup>. The most important aspect in the design of a diffuse reflector is the control of the ratio of specular and diffuse reflection for the designated purpose of use.

Metals easily satisfy the general requirements for diffuse reflectors with high reflectivity and low absorption. When it is flat and smooth, a metal surface reflects most of the incident light specularly with low diffuse reflection. Manipulation of a diffuse-reflective metal surface by a sputtering method has been reported<sup>86</sup>. One of good advantage of vacuum deposition is that a roughened surface can be directly created in the process. However, the process requires a high vacuum that is costly to procedure and not suitable for mass production.

Wet plating is a low cost and suitable for mass production of diffuse reflectors if the surface roughness of deposited metal can be controlled. It has been shown that PEM can be metallized to form metal nanoparticle/polymer composites or metal/polymer multilayered nanocomposites by electroless plating<sup>22,44,75</sup>. Our group previously

demonstrated the selective or non-selective electroless plating of self-assembled particle monolayers for opto-electronics applications<sup>22</sup>. Given by the fact that a non-selectively plated particle monolayer is uniformly rough over large areas due to the particles, we have investigated the possibility of using the surface as a diffuse reflector. Nickel is one of the most common electro-formed metals with moderate reflectivity along many wavelengths (Figure 10)<sup>87</sup>. When the reflectivity of nickel is less than what is expected, over-coating onto nickel surface by wet plating or a vacuum technique can provide better optical properties. For the higher industrial requirements of most applications today, metal reflectors are demanded to be heterogeneous or multilayered with further customizations. Further modifications include a brightening agent<sup>88,89</sup>, multilayering or over-coating<sup>90</sup>, and protective coating<sup>91,92</sup>. The nickel reflector is more cost-effective and efficient basis when a heterogeneous reflector is required.

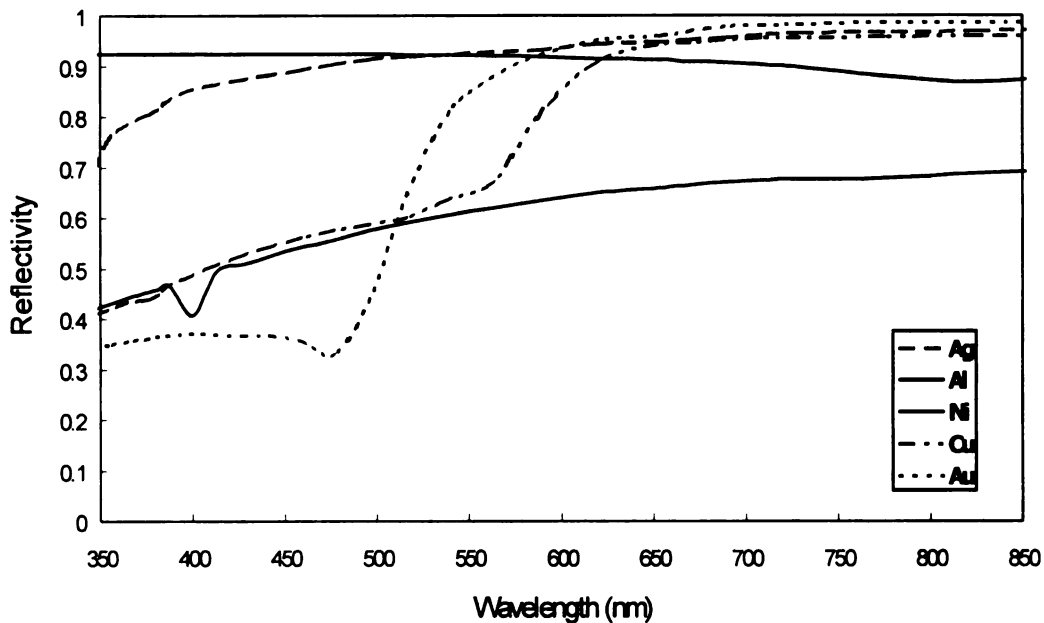


Figure 10: Reflectivity of Metals

To characterize the optical properties of the prepared diffuse reflectors, a phase angle optical microscope and a UV-VIS spectrometer with fiber optics and a scanning electron microscope are employed. Optical fibers permit versatile measurements for diffuse and specular reflectance of the sample.

## **3.2 Experimental Procedures**

Self-assembled particle monolayers were prepared by the same procedure described in Section, 2.2. Particles used in this study range from 140 nm to 5  $\mu\text{m}$ .

### **3.2.1 Electroless Plating of Particle Monolayers**

Two Pd based catalyst solutions were prepared using  $\text{Pd}(\text{NH}_4)_4\text{Cl}_2$  (catalysts 1) and  $\text{Na}_2\text{PdCl}_4$  (catalyst 2), each with a 5 mM concentration in deionized (DI) water. The samples of 2-D colloidal monolayers were immersed into two catalysts solutions consecutively for 10 sec (step 1). After washing with DI water followed by  $\text{N}_2$  drying, the pretreated samples were dipped into a Ni bath (step 2) for around 30 minutes. The electroless nickel bath contains nickel sulfate (Ni source, 4 g), sodium citrate (complexant, 2 g), lactic acid (buffer, complexant, 1g), and DMAB (reductant, 0.2g) in 100 ml of DI water. The pH of the Ni bath was adjusted to be 6.5 ( $\pm 0.1$ ) using ammonium hydroxide. For a particle free nickel surface, the same electroless plating method was applied to a polyelectrolyte coated substrate without particle monolayers atop. In this case, only the negative catalyst has been used and preloaded because topmost surface was positively charged PDAC.

### **3.2.2 Optical Characterizations of Diffuse Reflectors**

For microscopic images of the particle monolayers on surfaces, an optical

microscope (Nikon Eclipse ME600) and a Scanning Electron Microscope (JEOL 6400V with a LaB6 emitter) were used. To study the optical properties of the samples, a USB2000 fiber optic spectrometer from Ocean Optics was employed. All specular and diffuse reflectance spectra of the samples were referenced against high specular and diffuse reflectance standards purchased from Ocean Optics.

Figure 11 shows the measurement schematic for the specular and diffuse reflectance. To measure the specular reflectance the light source and the detecting probe are placed on opposite sides. Both the incident and reflecting angles were the same,  $45^\circ$ . For the diffuse reflectance the incident angle was  $75^\circ$  and the reflecting angle was  $45^\circ$ . Reflectance spectra were then averaged over the visible light range (400–500nm) to get averaged single values.

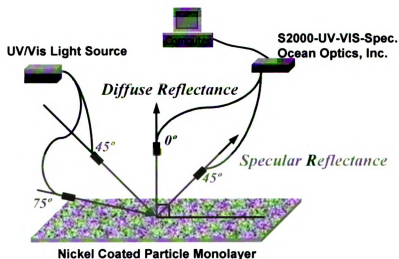


Figure 11: Measurement Schematic for Specular and Diffuse Reflectance

Figure 12 shows the scheme of measuring a distribution of light reflected from the sample surface. Incident angle was  $5^\circ$  and the mobile detecting probe was placed at different reflection angle ( $5^\circ$ – $90^\circ$ ) to acquire the angular dependent reflectance. All

reflectance intensities were measured at different angles, and averaged across visible light range. Average values were divided by the detector area resulting in flux density (i.e., number of photons per unit time and area). The flux densities at each angle were multiplied by the area calculated from the integration of an imaginary sphere at a given angle range. Once multiplied by the area, the flux densities were converted to flux (i.e., number of photons per unit time) and integration assumed that the distribution of light was hemispherical because the incident angle was close to  $0^\circ$ . The ratio of specularly and diffusively reflected light was derived from the distribution of reflected light. It was assumed that the specularly reflected light from the surface was populated in the region between  $0 \sim 3^\circ$  reflecting angle when incident light impinged the surface at an angle of  $5^\circ$ . The area of region in between the reflecting angle  $0\sim 3$  on the imaginary hemisphere was equivalent to that of the detector.

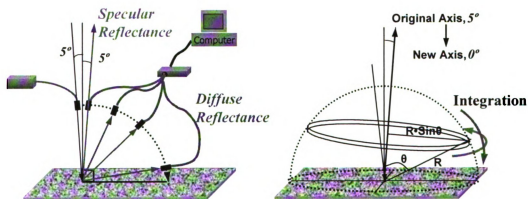


Figure 12: Measurement Schematics for Angular Dependent Reflectance

To compare the brightness from macroscopic view of the reflectors, a Nikon digital camera was employed. The reflectors were placed on a desk and photographed by varying the viewing angle to capture both the specularly and the diffusively reflected lights from a fluorescent lamp.

### 3.3 Results and Discussion

#### 3.3.1 Formation of Nickel Plated Particle Monolayers

Figure 13 shows the SEM image of a nickel-plated colloidal monolayer using 140 nm particles. As it was explained in Section 2.3.1, nanospheres (~100 nm) are adsorbed independently due to the same charge repulsion of the particles before the plating. During electroless plating the thick nickel metal layer growing on the surface of covered spherical particles on the substrate results in the development of hemispherical and irregular shapes. The thickness of nickel was comparable to the diameter of nanospheres used. Bigger particles appeared to be a merger or aggregates of two or more particles grown from a necking.

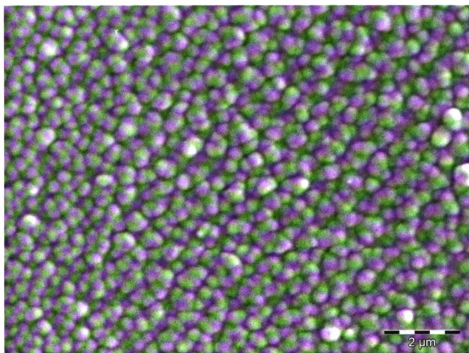


Figure 13: SEM Image of a Nickel-Plated 140 nm Particle Monolayer

Figure 14 shows the nickel-plated colloidal monolayer using 0.5 μm sized particles. Different from the nanospheres ( $D_{\text{particle}} \sim 100$  nm), microspheres ( $D_{\text{particle}} > 0.5$

$\mu\text{m}$ ) developed branch-like structures of clusters (see Figure 14). This image shows that spherical particles kept their shape but there were heavy neckings between particles due to the growth of nickel on the surface of the particles.

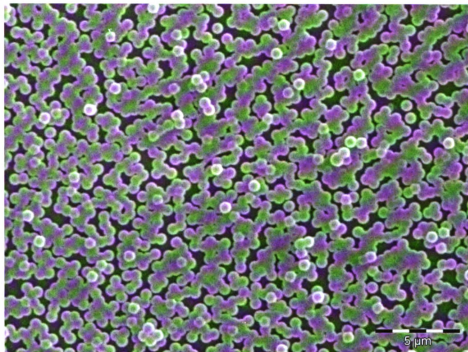


Figure 14: SEM Image of a Nickel-Plated 0.5  $\mu\text{m}$  Particle Monolayer

Figure 15 shows the optical microscopic image of the monolayer using 3  $\mu\text{m}$  particles. As shown in the Figure 15, long electroless plating develops crazes on the particle. As reported elsewhere, this is due to the internal stress build-up during electroless plating, which has been a great limitation of the process<sup>93,94</sup>. For optical reflector applications, there should be little transmittance of light through the electroformed reflectors. However, plating nickel over 30 minutes on the particle adsorbed surface results in the delamination of whole metal layer. Sometimes the crazed surface of nickel scatters more light in a diffuse reflection manner. However, when a thicker metal layer or composite multilayers are required the plating rate,

temperature, pH of bath solution, and selection of a different substrate for Ni plating should be optimized to lower internal stress<sup>93,94</sup>. It is notable that the electroformed nickel on a rough surface can bear greater internal stress than on a smooth surface at the same plating conditions. So we believe that particles incorporated into the nickel plating enhance the strength between nickel and the substrate, as demonstrated by Dr. Mackay, *et al.*<sup>95</sup>. This opens an interesting future work focusing on strengthening mechanical properties by the incorporation of nanoparticles or dendrimers during the plating process.

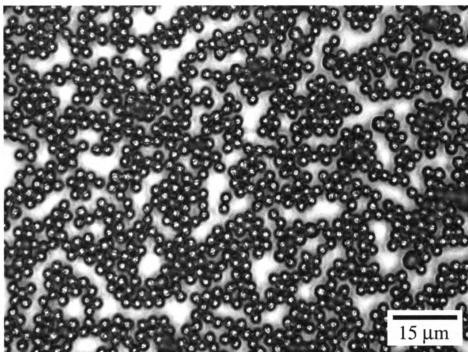


Figure 15: Optical Microscopic Image of Nickel-Plated 3  $\mu\text{m}$  Particle Monolayer

### 3.3.2 Optical Characterizations of Diffuse Reflectors

Figure 16 shows the average specular and diffuse reflectances as a function of particle size. The average specular reflectance decreases and the average diffuse reflectance increases along with the increase in particle size. Since the measured

reflectances are referenced against the high specular standard, the specular reflectance 38.09 % of 0.14  $\mu\text{m}$  sample is the highest. The samples made of particles greater than 3  $\mu\text{m}$  have values of the specular reflectance less than 0.6 %.

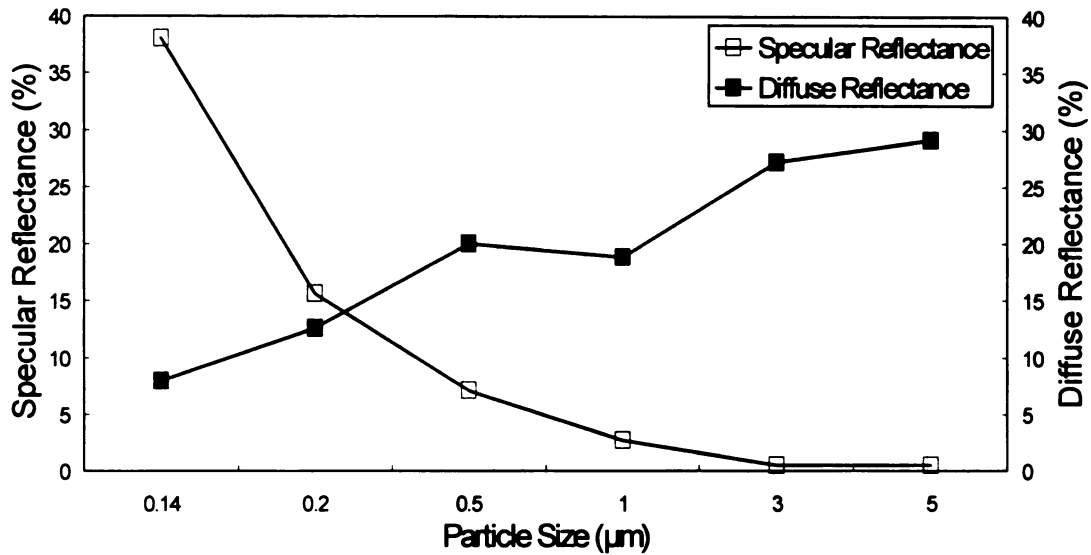


Figure 16: Specular and Diffuse Reflectance

Figure 17 shows the distribution of lights reflected from the sample surfaces, converted from the integration of angular dependent reflectance. When the incident angle is  $5^\circ$ , specularly reflected light is in between  $0 \sim 3^\circ$  on the graph. It turns out that the reflectors using this method don't produce a focused reflection. Instead, the reflectors reflect lights randomly in all directions.

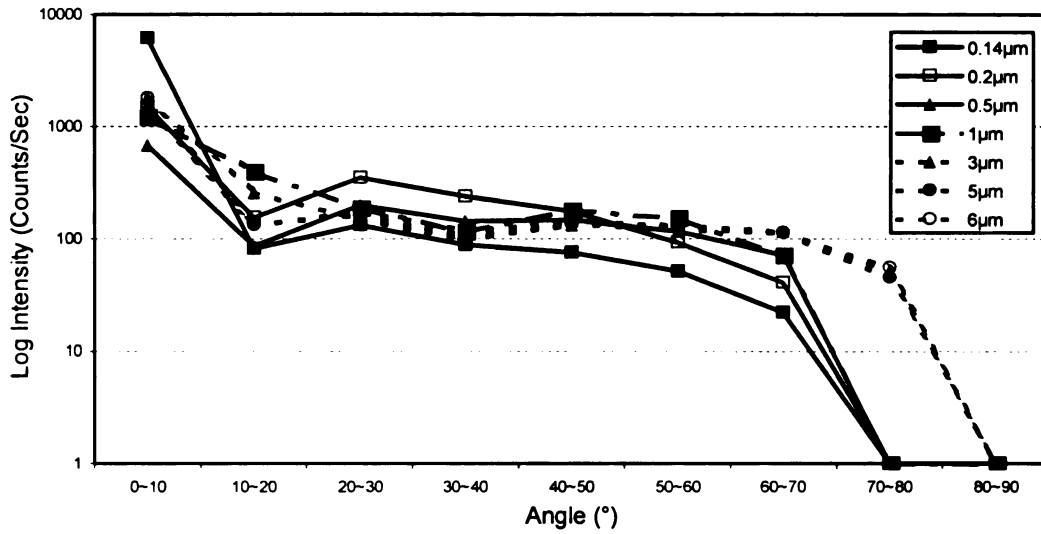


Figure 17: Distribution of Reflected Light

From the reflected light distribution study, the ratio of the specular and diffuse reflection at the incident angle of  $5^\circ$  was derived and tabulated in Table 2. The result shows that the samples can control the amount of specular reflection from  $\sim 50$  to  $90\%$  by only changing the size of the particles. Table 2 provides a guideline to select a size of the particle used for a required amount of diffuse reflectance for the purpose.

Table 2: Ratio of Specular and Diffuse Reflection

Particle Size ( $\mu\text{m}$ )	0.14	0.2	0.5	1	3	5
Specular Reflection (%)	91.75	57.66	45.38	43.52	40.03	40.79
Diffuse Reflection (%)	8.25	42.34	54.62	56.48	59.97	59.21

Figure 18 shows two macroscopic images of reflectors taken by a digital camera

at different angles. The size of particles is increasing from left to right and the brightness of the specular (upper) and the diffuse reflections (lower) is inversely changing along with the increase in particle size. Particle free or nanosphere monolayers (left) are brighter in specular reflection and darker in diffuse reflection than bigger particle monolayers (right). It is because they (left) are reflecting most of the lights in a specular reflection as calculated in Table 1. On the other hand, samples with microspheres (right) are darker under the specular reflection condition and brighter under the diffuse reflection condition because they reflect about half of incident lights specularly and the other half diffusively.

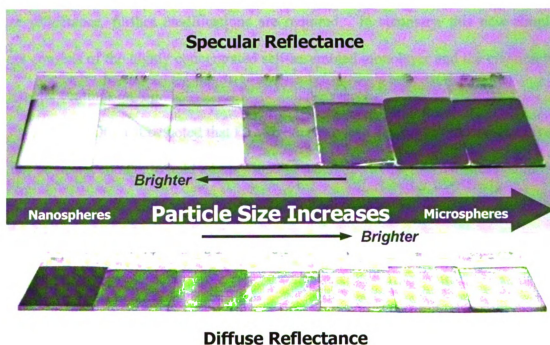


Figure 18: Macroscopic View of Reflectors at Different Angles

### 3.4 Conclusions

We have developed a novel fabrication method of diffuse reflectors. Tuning of

the specular and diffuse reflectance has been easily achieved by changing the size of particles. The new process is cost-effective and convenient for mass production due to the simple immersion steps without the need of a high vacuum. Depending on the required optical property, this method can be combined with the additional over-coatings of different metals such as aluminum or silver by wet plating or a vacuum technique<sup>90</sup>. However, the vacuum deposition technique will decrease the production yield and increase the processing cost as well.

The portion of specularly reflected light from the total reflected light ranged from 50 to 90% as a function of particle size. To decrease specular reflection or to increase diffuse reflectance, further modifications are required. In summary, this new simple process consists of the highly concentrated self-assembled monolayer and the creation of rough metal coatings on top.

However, it must be noted that PEM binder between a substrate and a metal layer may not be strong enough to hold a heavy load of metal due to the internal stress build-up. When a strong binder is required, annealing of electroformed metals<sup>93,94</sup> or silane modified surfaces as a covalently adhesive layer can be considered<sup>30</sup>. The stability or durability of the prepared metal-polymer reflectors remains as a future investigation.

## 4. Summary and Conclusions

We have studied the functional PS particle size effects on the formations, structures, and optical properties on PEM-coated glass slides. The particles formed RCP or dispersed particle monolayers that deposited on the substrate by electrostatic attraction forces and then rearranged by capillary forces among the attached monolayer particles. Compared to other particle deposition approaches, the overall procedure used in this work was very simple, cost-effective, and environmentally friendly. The total transmittance, measured using an IS detector, remained unchanged along with the particle sizes and conversely the specular transmittance, measured using a PMT detector, changed considerably. No significant reflection or absorption by the coated monolayer has been found. This indicates that the incident visible light optically interacts with the particle monolayers through optical interference, diffraction, and/or scattering events. Three main optical characteristics as a ratio of particle diameter vs. wavelength of incident beam ( $D/\lambda$ ) are the following: (a) Anti-reflection (when  $D/\lambda \sim 0.25$ ), (b) diffraction (when  $D/\lambda \sim 1$ ), and (c) diffusive scattering (when,  $D/\lambda > 1$ ). We believe this study is important in that the work includes fundamental colloidal behavior and provides functional optical coatings available for the further modifications.

The coatings were further plated with nickel by a two-step electroless plating technique with two palladium catalysts. Using these demonstrated new steps we have developed a novel method of creating diffusive metal reflectors. This newly proposed method can remove the vacuum procedures and provide a low cost process without special equipment. Optical characterizations revealed that the reflector can reduce the

specular reflectance and enhance the diffuse reflectance by only changing the size of the particles used. Angular dependent measurements and integrations step successfully demonstrated how to derive the distribution of reflected light and the ratio of the specular and diffuse reflections from the total reflected lights. This method is also available for further customizations including changing adhesive layer, incorporation of other molecules, over-coating of other metals, and heat treatment to enhance the optical performance. We believe this study opens a way to fabricate more complex systems and to perform various future works, and can be further used as templates for selective and non-selective metal plating<sup>75</sup>, cell adhesion<sup>76</sup>, and quantum dot deposition<sup>7</sup>.

## 5. Bibliography

1. Park, S. H. & Xia, Y. Assembly of mesoscale particles over large areas and its application in fabricating tunable optical filters. *Langmuir* **15**, 266-273 (1999).
2. Rogach, A. et al. Nano- and microengineering. Three-dimensional colloidal photonic crystals prepared from submicrometer-sized polystyrene latex spheres pre-coated with luminescent polyelectrolyte/nanocrystal shells. *Advanced Materials (Weinheim, Germany)* **12**, 333-337 (2000).
3. Lopez, C. Materials aspects of photonic crystals. *Advanced Materials (Weinheim, Germany)* **15**, 1679-1704 (2003).
4. Xia, Y., Gates, B., Yin, Y. & Lu, Y. Monodispersed colloidal spheres: Old materials with new applications. *Advanced Materials (Weinheim, Germany)* **12**, 693-713 (2000).
5. Fustin, C.-A., Glasser, G., Spiess, H. W. & Jonas, U. Site-selective growth of colloidal crystals with photonic properties on chemically patterned surfaces. *Advanced Materials (Weinheim, Germany)* **15**, 1025-1028 (2003).
6. Zhao, Y. et al. The fabrication of photonic band gap materials with a two-dimensional defect. *Applied Physics Letters* **82**, 3764-3766 (2003).
7. Wang, D., Rogach, A. L. & Caruso, F. Composite Photonic Crystals from Semiconductor Nanocrystal/Polyelectrolyte-Coated Colloidal Spheres. *Chem. Mater.* **15**, 2724 -2729 (2003).
8. Jiang, P., Bertone, J. F., Hwang, K. S. & Colvin, V. L. Single-Crystal Colloidal Multilayers of Controlled Thickness. *Chemistry of Materials* **11**, 2132-2140 (1999).
9. Hattori, H. Anti-reflection surface with particle coating deposited by electrostatic attraction. *Advanced Materials* **13**, 51-+ (2001).
10. Kumar, A. & Whitesides, G. M. Patterned Condensation Figures as Optical Diffraction Gratings. *Science, New Series* **263**, 60-62 (1994).
11. Burch, J. M. *Nature* **171**, 889-890 (1953).
12. Wu, M.-H. & Whitesides, G. M. Fabrication of arrays of two-dimensional micropatterns using microspheres as lenses for projection photolithography. *Applied Physics Letters* **78**, 2273-2275 (2001).
13. Burmeister, F. et al. Colloid Monolayers as Versatile Lithographic Masks.

- Langmuir* **13**, 2983-2987 (1997).
14. Burmeister, F. et al. From mesoscopic to nanoscopic surface structures. Lithography with colloid monolayers. *Chemical Engineering & Technology* **21**, 761-763 (1998).
  15. Takei, H. Surface-adsorbed polystyrene spheres as a template for nanosized metal particle formation: Optical properties of nanosized Au particle. *Journal of Vacuum Science & Technology, B: Microelectronics and Nanometer Structures* **17**, 1906-1911 (1999).
  16. Zheng, H., Lee, I., Rubner, M. F. & Hammond, P. T. Two component particle arrays on patterned polyelectrolyte multilayer templates. *Advanced Materials (Weinheim, Germany)* **14**, 569-572 (2002).
  17. Lee, I., Zheng, H., Rubner, M. F. & Hammond, P. T. Controlled cluster size in patterned particle arrays via directed adsorption on confined surfaces. *Advanced Materials (Weinheim, Germany)* **14**, 572-577 (2002).
  18. Brisson, V. & Tilton, R. D. Self-assembly and two-dimensional patterning of cell arrays by electrophoretic deposition. *Biotechnology and Bioengineering* **77**, 290-295 (2002).
  19. Yin, Y., Lu, Y. & Xia, Y. Assembly of monodispersed spherical colloids into one-dimensional aggregates characterized by well-controlled structures and lengths. *Journal of Materials Chemistry* **11**, 987-989 (2001).
  20. Aizenberg, J., Braun, P. V. & Wiltzius, P. Patterned Colloidal Deposition Controlled by Electrostatic and Capillary Forces. *Physical Review Letters* **84**, 2997-3000 (2000).
  21. Masuda, Y., Itoh, M., Yonezawa, T. & Koumoto, K. Low-Dimensional Arrangement of SiO<sub>2</sub> Particles. *Langmuir* **18**, 4155-4159 (2002).
  22. Lee, I., Hammond, P. T. & Rubner, M. F. Selective Electroless Nickel Plating of Particle Arrays on Polyelectrolyte Multilayers. *Chemistry of Materials* **15**, 4583-4589 (2003).
  23. Liu, F.-K., Chang, Y.-C., Ko, F.-H., Chu, T.-C. & Dai, B.-T. Rapid fabrication of high quality self-assembled nanometer gold particles by spin coating method. *Microelectronic Engineering* **67-68**, 702-709 (2003).
  24. Dimitrov, A. S. & Nagayama, K. Continuous Convective Assembling of Fine Particles into Two-Dimensional Arrays on Solid Surfaces. *Langmuir* **12**, 1303-1311 (1996).
  25. Picard, G., Nevernov, I., Alliata, D. & Pazdernik, L. Dynamic Thin Laminar Flow Method for Making Protein Monolayers. *Langmuir* **13**, 264-276 (1997).

26. Hayward, R. C., Saville, A. & Aksay, A. Electrophoretic assembly of colloidal crystals with optically tunable micropatterns. *Nature (London)* **404**, 56-59 (2000).
27. Denkov, N. et al. Mechanism of formation of two-dimensional crystals from latex particles on substrates. *Langmuir* **8**, 3183-3190 (1992).
28. Taniguchi, T., Shinohara, S., Kawaguchi, S. & Nagai, K. Fabrication of self-assembled polymer particle monolayers on gold substrates. *Chemistry Letters (Japan)*, 1180-1181 (2002).
29. Malikova, N., Pastoriza-Santos, I., Schierhorn, M., Kotov, N. A. & Liz-Marzan, L. M. Layer-by-Layer Assembled Mixed Spherical and Planar Gold Nanoparticles: Control of Interparticle Interactions. *Langmuir* **18**, 3694-3697 (2002).
30. Sato, T., Hasko, D. G. & Ahmed, H. Nanoscale colloidal particles: monolayer organization and patterning. *Journal of Vacuum Science & Technology, B: Microelectronics and Nanometer Structures* **15**, 45-48 (1997).
31. Bar, G., Rubin, S., Cutts, R. W., Taylor, T. N. & Zawodzinski, T. A., Jr. Dendrimer-Modified Silicon Oxide Surfaces as Platforms for the Deposition of Gold and Silver Colloid Monolayers: Preparation Method, Characterization, and Correlation between Microstructure and Optical Properties. *Langmuir* **12**, 1172-9 (1996).
32. Serizawa, T., Takeshita, H. & Akashi, M. Electrostatic Adsorption of Polystyrene Nanospheres onto the Surface of an Ultrathin Polymer Film Prepared by Using an Alternate Adsorption Technique. *Langmuir* **14**, 4088-4094 (1998).
33. Himmelhaus, M. & Takei, H. Self-assembly of polystyrene nanoparticles into patterns of random-close-packed monolayers via chemically induced adsorption. *Physical Chemistry Chemical Physics* **4**, 496-506 (2002).
34. Kralchevsky, P. A. & Nagayama, K. Capillary forces between colloidal particles. *Langmuir* **10**, 23-36 (1994).
35. Rakers, S., Chi, L. F. & Fuchs, H. Influence of the Evaporation Rate on the Packing Order of Polydisperse Latex Monofilms. *Langmuir* **13**, 7121-7124 (1997).
36. Decher, G. & Hong, J.-D. Buildup of ultrathin multilayer films by a self-assembly process, (1) consecutive adsorption of anionic and cationic bipolar amphiphiles on charged surfaces. *Makromol Chem Macromol Symp.* **46**, 321-327 (1991).
37. Decher, G. & Hong, J. D. Buildup of Ultrathin Multilayer Films by a Self-Assembly Process .2. Consecutive Adsorption of Anionic and Cationic Bipolar Amphiphiles and Polyelectrolytes on Charged Surfaces. *Berichte Der Bunsen-Gesellschaft-Physical Chemistry Chemical Physics* **95**, 1430-1434 (1991).
38. Decher, G. Fuzzy nanoassemblies: toward layered polymeric multicomposites.

- Science* **277**, 1232 (1997).
39. Hammond, P. T. Recent explorations in electrostatic multilayer thin film assembly. *Current Opinion in Colloid & Interface Science* **4**, 430-442 (2000, Volume Date 1999).
  40. Chodanowski, P. & Stoll, S. Polyelectrolyte adsorption on charged particles: Ionic concentration and particle size effects-A Monte Carlo approach. *Journal of Chemical Physics* **115**, 4951-4960 (2001).
  41. Caruso, F., Lichtenfeld, H., Donath, E. & Mohwald, H. Investigation of Electrostatic Interactions in Polyelectrolyte Multilayer Films: Binding of Anionic Fluorescent Probes to Layers Assembled onto Colloids. *Macromolecules* **32**, 2317-2328 (1999).
  42. Welch, P. & Muthukumar, M. Dendrimer-Polyelectrolyte Complexation: A Model Guest-Host System. *Macromolecules* **33**, 6159-6167 (2000).
  43. Jessel, N. et al. Bioactive Coatings Based on a Polyelectrolyte Multilayer Architecture Functionalized by embedded Proteins. *Advanced Materials (Weinheim, Germany)* **15**, 692-695 (2003).
  44. Wang, T. C., Cohen, R. E. & Rubner, M. F. Metallodielectric photonic structures based on polyelectrolyte multilayers. *Advanced Materials (Weinheim, Germany)* **14**, 1534-1537 (2002).
  45. Bertrand, P., Jonas, A., Laschewsky, A. & Legras, R. Ultrathin polymer coatings by complexation of polyelectrolytes at interfaces: suitable materials, structure and properties. *Macromolecular Rapid Communications* **21**, 319-348 (2000).
  46. Khopade, A. J. & Caruso, F. Investigation of the Factors Influencing the Formation of Dendrimer/Polyanion Multilayer Films. *Langmuir* **18**, 7669-7676 (2002).
  47. He, J.-A. et al. Electrostatic Multilayer Deposition of a Gold-Dendrimer Nanocomposite. *Chemistry of Materials* **11**, 3268-3274 (1999).
  48. Cant, N. E. et al. Fabrication and Characterization of Self-Assembled Nanoparticle/Polyelectrolyte Multilayer Films. *Journal of Physical Chemistry B* **107**, 13557-13562 (2003).
  49. Caruso, F., Spasova, M., Salgueirino-Maceira, V. & Liz-Marzan, L. M. Multilayer assemblies of silica-encapsulated gold nanoparticles on decomposable colloid templates. *Advanced Materials (Weinheim, Germany)* **13**, 1090-1094 (2001).
  50. Ferreyra, N., Coche-Guerente, L., Fatisson, J., Lopez Teijelo, M. & Labbe, P. Layer-by-layer self-assembled multilayers of redox polyelectrolytes and gold nanoparticles. *Chemical Communications (Cambridge, United Kingdom)*, 2056-

- 2057 (2003).
51. Kidambi, S., Dai, J., Li, J. & Bruening, M. L. Selective Hydrogenation by Pd Nanoparticles Embedded in Polyelectrolyte Multilayers. *Journal of the American Chemical Society* **126**, 2658-2659 (2004).
  52. Lvov, Y., Ariga, K., Onda, M., Ichinose, I. & Kunitake, T. Alternate Assembly of Ordered Multilayers of SiO<sub>2</sub> and Other Nanoparticles and Polyions. *Langmuir* **13**, 6195-6203 (1997).
  53. Schrof, W. et al. Nonlinear optical properties of polyelectrolyte thin films containing gold nanoparticles investigated by wavelength dispersive femtosecond degenerate four wave mixing (DFWM). *Advanced Materials (Weinheim, Germany)* **10**, 338-341 (1998).
  54. Wang, T. C., Rubner, M. F. & Cohen, R. E. Manipulating Nanoparticle Size within Polyelectrolyte Multilayers via Electroless Nickel Deposition. *Chemistry of Materials* **15**, 299-304 (2003).
  55. Picart, C. et al. Determination of structural parameters characterizing thin films by optical methods: A comparison between scanning angle reflectometry and optical waveguide lightmode spectroscopy. *Journal of Chemical Physics* **115**, 1086-1094 (2001).
  56. Ostrander, J. W., Mamedov, A. A. & Kotov, N. A. Two Modes of Linear Layer-by-Layer Growth of Nanoparticle-Polyelectrolyte Multilayers and Different Interactions in the Layer-by-layer Deposition. *Journal of the American Chemical Society* **123**, 1101-1110 (2001).
  57. Lvov, Y., Ariga, K., Ichinose, I. & Kunitake, T. Assembly of Multicomponent Protein Films by Means of Electrostatic Layer-by-Layer Adsorption. *Journal of the American Chemical Society* **117**, 6117-23 (1995).
  58. van Duffel, B., Ras, R. H. A., De Schryver, F. C. & Schoonheydt, R. A. Langmuir-Blodgett deposition and optical diffraction of two-dimensional opal. *Journal of Materials Chemistry* **11**, 3333-3336 (2001).
  59. Szekeres, M. et al. Ordering and optical properties of monolayers and multilayers of silica spheres deposited by the Langmuir-Blodgett method. *Journal of Materials Chemistry* **12**, 3268-3274 (2002).
  60. Barnsley, M. *Fractals Everywhere, Ch. 5* (Academic Press, Inc., Boston, 1988).
  61. Semmler, M., Mann, E. K., Ricka, J. & Borkovec, M. Diffusional deposition of charged latex particles on water-solid interfaces at low ionic strength. *Langmuir* **14**, 5127-5132 (1998).
  62. Chen, K. M., Jiang, X., Kimerling, L. C. & Hammond, P. T. Selective Self-

- Organization of Colloids on Patterned Polyelectrolyte Templates. *Langmuir* **16**, 7825-7834 (2000).
63. Hinrichsen, E. L., Feder, J. & Jossang, T. *Physical Review Letters* **44**, 793 (1986).
  64. Feder, J. *Journal of Theor. Biol.* **87**, 237 (1980).
  65. Meakin, P. Models for colloidal aggregation. *Annual Review of Physical Chemistry* **39**, 237-267 (1988).
  66. Lattuada, M., Wu, H. & Morbidelli, M. A simple model for the structure of fractal aggregates. *Journal of Colloid and Interface Science* **268**, 106-120 (2003).
  67. Hiemenz, P. C. & Rajagopalan, R. *Principles of colloid and Surface Chemistry* (Marcel Dekker, New York, 1997).
  68. Lin, M. Y. et al. Universality in colloid aggregation. *Nature* **339**, 360 - 362 (1989).
  69. Krieger, I. M. & O'Neill, F. M. Diffraction of light by arrays of colloidal spheres. *Journal of the American Chemical Society* **90**, 3114-20 (1968).
  70. Born, M. & Wolf, E. *Principles of Optics: Electromagnetics Theory of Propagation, Interference and Diffraction of Light, 4th Edn.* (Pergamon, Oxford, 1970).
  71. Walheim, S., Schaffer, E., Mlynek, J. & Steiner, U. Nanophase-separated polymer films as high-performance antireflection coatings. *Science (Washington, D. C.)* **283**, 520-522 (1999).
  72. Neuman, G. A. & Glass Technology Center, P. I. I., Pittsburgh, PA, USA. Anti-reflective coatings by APCVD using graded index layers. *Journal of Non-Crystalline Solids* **218**, 92-99 (1997).
  73. Szczyrbowski, J., Braeuer, G., Teschner, G., Zmelty, A. & Leybold Systems GmbH, W.-R.-S., Hanau, Germany. Antireflective coatings on large scale substrates produced by reactive twin-magnetron sputtering. *Journal of Non-Crystalline Solids* **218**, 25-29 (1997).
  74. Yagi, Y., Matsushita, S. I., Tryk, D. A., Koda, T. & Fujishima, A. Observation of Light Propagation in Single Layers of Composite Two-Dimensional Arrays. *Langmuir* **16**, 1180-1184 (2000).
  75. Wang, T. C., Chen, B., Rubner, M. F. & Cohen, R. E. Selective Electroless Nickel Plating on Polyelectrolyte Multilayer Platforms. *Langmuir* **17**, 6610-6615 (2001).
  76. Yang, S. Y., Mendelsohn, J. D. & Rubner, M. F. New Class of Ultrathin, Highly Cell-Adhesion-Resistant Polyelectrolyte Multilayers with Micropatterning Capabilities. *Biomacromolecules* **4**, 987-994 (2003).

77. Wei, C.-k. in *U.S.* 7 pp. ((Industrial Technology Research Institute, Taiwan). Us, 1997).
78. Kretman, W. D. & Kaytor, S. R. in *U.S.* 28 pp., Cont.-in-part of U. S. 5,976,686. ((3M Innovative Properties Company, USA). Us, 2002).
79. Sakamoto, M., Yamaguchi, Y., Ikeno, H., Matsuno, F. & Kikkawa, H. in *Eur. Pat. Appl.* ((NEC Corporation, Japan). Ep, 2002).
80. Banerjee, A. & Guha, S. Study of back reflectors for amorphous silicon alloy solar cell application. *Journal of Applied Physics* **69**, 1030-5 (1991).
81. Cotter, J. E. Optical intensity of light in layers of silicon with rear diffuse reflectors. *Journal of Applied Physics* **84**, 618-624 (1998).
82. Fedders, P. A. Surface roughness and the absorption of electromagnetic waves in simple metals. *Physical Review* **181**, 1053-8 (1969).
83. Fuelleman, R., Mauser, R., Specht, M., Stauch, H. & Oelkrug, D. Time- and angle resolved reflection spectroscopy of the oxide layer formation on metal surfaces. *Journal of Molecular Structure* **143**, 251-4 (1986).
84. West, C. S. & O'Donnell, K. A. Angular correlation functions of light scattered from weakly rough metal surfaces. *Physical Review B: Condensed Matter and Materials Physics* **59**, 2393-2406 (1999).
85. Roos, A., Bergkvist, M., Ribbing, C. G. & Bennett, J. M. Quantitative interface roughness studies of copper oxide on copper. *Thin Solid Films* **164**, 5-11 (1988).
86. Kamoshida, K. Preparation of low-reflectivity aluminum film using direct current magnetron sputtering in Ar/O<sub>2</sub> and Ar/N<sub>2</sub> atmospheres. *Journal of Vacuum Science & Technology, B: Microelectronics and Nanometer Structures* **18**, 2565-2568 (2000).
87. Lide, D. R. *CRC Handbook of Chemistry and Physics* (CRC Press, 1991).
88. Nikolic, N. D., Rakocevic, Z. & Popov, K. I. Structural characteristics of bright copper surfaces. *Journal of Electroanalytical Chemistry* **514**, 56-66 (2001).
89. Nikolic, N. D., Rakocevic, Z., Durovic, D. R. & Popov, K. I. Reflection and structural characteristics of semi-bright and mirror bright nickel coatings. *Journal of the Serbian Chemical Society* **67**, 437-443 (2002).
90. Zhang, Q.-C. & Mills, D. R. Very low-emittance solar selective surfaces using new film structures. *J. Appl. Phys.* **72**, 3013 (1992).
91. Dimant, A. B. et al. in *Fr. Demande* 19 pp. ((Scientific-Research and Experimental Institute of Motor-Vehicle Electrical Equipment and Instruments,

USSR). Fr, 1981).

92. Okitsu, H. in *Jpn. Kokai Tokkyo Koho* 5 pp. ((Toshiba Glass Co., Ltd., Japan). Jp, 1999).
93. Song, J. Y. & Yu, J. Residual stress measurements in electroless plated Ni-P films. *Thin Solid Films* **415**, 167-172 (2002).
94. Martyak, N. M. Counterion effects during electroless nickel plating. *Metal Finishing* **101**, 41-47 (2003).
95. Mackay, M. E. et al. Nanoscale effects leading to non-Einstein-like decrease in viscosity. *Nature Materials* **2**, 762-766 (2003).

MICHIGAN STATE UNIVERSITY LIBRARIES



3 1293 02497 7112